🔓**Open Access**
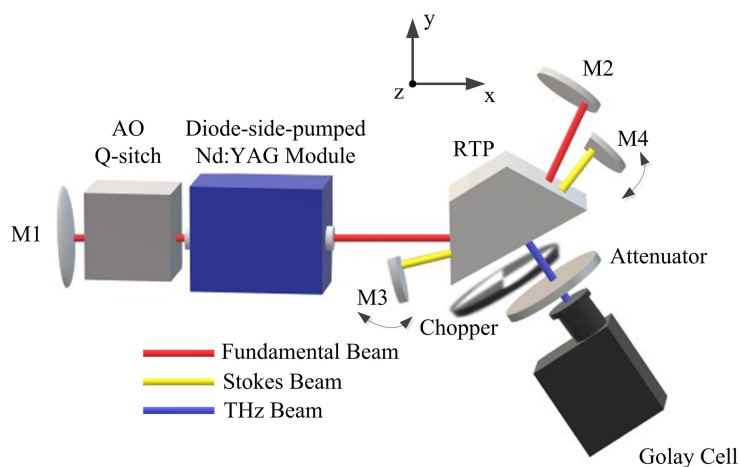
High Average Power Diode-Side-Pumped Intracavity Terahertz Parametric Source Based on Stimulated Polariton Scattering in RbTiOPO₄ Crystal

Feilong Gao
Xingyu Zhang
Zhenhua Cong
Zhaojun Liu
Xiaohan Chen
Zengguang Qin
Peng Wang
Jinjin Xu
Weitao Wang
Shaojun Zhang

High Average Power Diode-Side-Pumped Intracavity Terahertz Parametric Source Based on Stimulated Polariton Scattering in RbTiOPO$_4$ Crystal

Feilong Gao,[1] **Xingyu Zhang,**[1] **Zhenhua Cong,**[1] **Zhaojun Liu,**[1]
Xiaohan Chen,[1] **Zengguang Qin,**[1] **Peng Wang,**[1] **Jinjin Xu,**[1]
Weitao Wang,[2] **and Shaojun Zhang**[3]

[1]School of Information Science and Engineering, Shandong Provincial Key Laboratory of Laser Technology and Application, Shandong University, Qingdao 266237, China
[2]Laser Institute of Shandong Academy of Sciences, Jinan 250014, China
[3]State Key Laboratory of Crystal Materials, Shandong University, Jinan 250100, China

Abstract: This paper reports an intracavity terahertz parametric source based on the stimulated polariton scattering in RbTiOPO$_4$ crystal with a high repetition rate and a high average power. The side pumping for the gain medium by laser diodes is adopted to get a higher fundamental power and a larger fundamental laser beam size than those in the diode-end-pumping in order to improve the THz output power. A non-collinear convex-plane fundamental cavity is adopted so that the thermal effect can be offset in some degree and the fundamental beam size is further increased. The obtained maximum average THz output power is 367 μW at 3.88 THz when the diode pump power is 105 W and the pulse repetition frequency (PRF) is 7 kHz. The terahertz power of 367 μW is the highest ever obtained in SPS sources.

Index Terms: Nonlinear optics, THz sources, stimulated polariton scattering.

1. Introduction

Terahertz wave sources have received considerable attention for many applications such as material science, drug and food inspection, security checking, biomedicine, and imaging [1]–[6]. Stimulated polariton scattering (SPS) is an efficient nonlinear effect which can be used to generate the terahertz wave. It is a mixed second-order and third-order nonlinear process. When a sufficiently strong fundamental laser is incident in polar crystals (both infrared-active and Raman-active), a near-infrared wave (which is usually called Stokes wave) and a far-infrared wave at THz frequency are parametrically generated. The systems based on the SPS effect are usually compact and low cost, and operated at room-temperature. The generated THz radiation is highly coherent in time and space and widely frequency-tunable. In the SPS process, the fundamental, Stokes and THz waves must follow the momentum conservation and energy conservation laws [8].

In the past more than twenty years, the nonlinear crystals used in the SPS sources are usually $LiNbO_3$ or $MgO:LiNbO_3$ (MgO:LN), and the frequency range of the THz wave is from 0.5 to 3.6 THz [9]–[13]. In recent years, some researches have been conducted to expand the tuning range of the THz frequency by using crystals besides $LiNbO_3$, such as $KTiOPO_4$ (KTP), $KTiOAsO_4$ (KTA), and $RbTiOPO_4$ (RTP) [14]–[16]. RTP crystal is an excellent nonlinear crystal. Its nonlinear coefficient is large ($d_{33} = 15.6$ pm/V) [17]. Compared with MgO:LN, KTP, and KTA, the RTP crystal has higher optical damage threshold (15 J/cm^2 at 10 Hz, 6 ns, 1064 nm) [18]. Higher optical damage threshold improves the performance of bearing higher pump power. RTP has better performance in SPS lasers than MgO:LN, KTP and KTA [16], [19], [20].

According to the position of the nonlinear crystal, SPS sources include external-cavity pumped systems and intracavity pumped systems. The external-cavity pumped systems are mainly used to generate terahertz pulses with relatively high pulse energies and low pulse repetition rates [21]–[23]. In the intracavity pumped systems, nonlinear crystals are inserted into the fundamental cavity so that it can take advantage of the high intracavity fundamental power to reach the SPS threshold under relatively low diode pump power. Compared with external-cavity pumped systems, the intracavity pumped SPS sources are usually more compact and exhibit relatively low SPS threshold, high terahertz pulse repetition rate, high THz output power, and high diode-to-THz efficiency.

Over the past decade, nearly all the reported intracavity SPS systems adopted the diode-end-pumped configuration. In 2006, T. J. Edwards *et al.* demonstrated a diode-end-pumped intracavity SPS system based on the MgO:LN crystal. The generated THz pulse energy was 5 nJ at 1.6 THz when the repetition rate was 15 Hz (implying mean power of 75 nW) [24]. In 2008, D. J. M. Stothard *et al.* improved the THz radiation power by increasing the repetition rate. The THz pulse energy was 30 nJ at a repetition rate up to 400 Hz (implying mean power of 12 μW) [25]. In 2013, A. J. Lee reported an intracavity, diode-end-pumped THz source based on the MgO:LN crystal. The obtained average THz power was 6.45 μW at 1.82 THz under the diode power of 5 W [26]. In 2016, T. A. Ortega reported an intracavity SPS source using a linear RTP crystal in the Si-prism array coupler configuration. The average THz power was 16.2 μW at 3.8 THz [16]. In 2017, T. A. Ortega improved the performance of the SPS laser by coating a Teflon thin film on the THz reflection surface of the MgO:LN crystal in the surface-emitted (SE) configuration. The optical damage threshold of the MgO:LN surface was then increased, and the THz output power was detected as 56.8 μW at 1.76 THz under the diode pump power of 6.5 W [27]. In 2018, T. A. Ortega reported an intracavity SPS source using the RTP crystal in the SE configuration. The maximum THz output power was detected as 124.7 μW at 4.10 THz under the diode power of 6.0 W. So far, the THz power of 124.7 μW is the highest level for intracavity SPS sources [19].

In the diode-end-pumped configuration, the intracavity fundamental beam couples efficiently with the diode pump beam, which results in low laser threshold and high diode-to-fundamental and then high diode-to-THz conversion efficiencies. However, there are some limiting factors for further improving the average THz output power. Firstly, in the SPS process, the generations of the Stokes and THz waves arise from the consumption of the fundamental wave. It means that for a certain nonlinear crystal, the parametric process has a positive correlation with the fundamental wave power. In the diode-end-pumped systems, the diode pump power and then intracavity fundamental power are limited by the thermal fracture of the laser material [28]. Thermally induced spherical aberration and birefringence can also significantly degrade the laser performance [29]. Secondly, the fundamental beam size in the end-pumped configuration is usually small (usually several hundred micrometers). Because the refractive index of nonlinear crystals to THz wave is large, the SPS process must follow the non-collinear phase matching condition [8] (see Fig. 1). Larger fundamental beam size means larger nonlinear interaction volume among the fundamental, Stokes and terahertz beams. So, increasing the fundamental pump power and fundamental beam size are effective measures to improve the THz output power. Diode-side-pumping for the fundamental laser gain medium is a good solution. In the diode-side-pumped intracavity configurations, because the distribution of the diode pump wave in the laser medium is uniform, the thermal effect is relatively light. As a result, the systems can work efficiently even under high diode pump power [30]. In
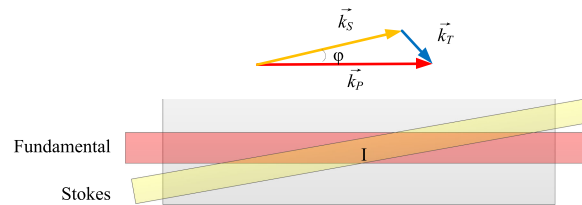
Fig. 1. The non-collinear phase-matching condition, and the overlapping area between fundamental and stokes beams in the crystal.
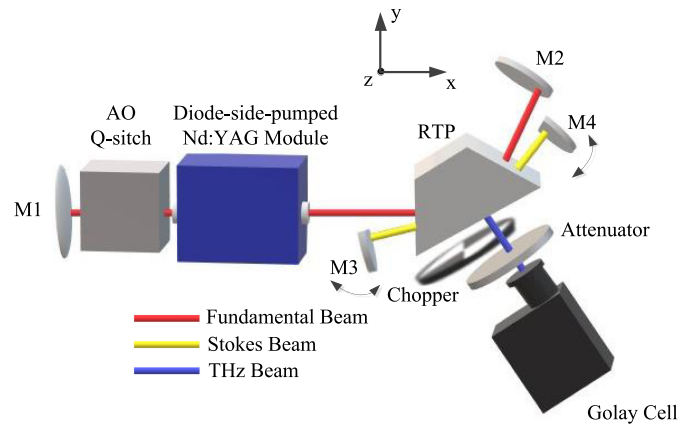

Fig. 2. Experimental setup of the intracavity RTP SPS laser adopting the diode-side-pumped configuration.

addition, the fundamental beam size is relatively large [31]. The diode-side-pumped configuration has been used to generate high output power in some fields [32]–[36]. Of course it should be pointed out that the diode-side-pumped systems have the common disadvantage that the optical-to-optical efficiency is lower due to the insufficient absorption of the diode pump light in the outer part of the laser rod.

With a desire to achieve a SPS laser with high repetition rate and high average power, we employed the intracavity diode-side-pumped configuration in a RTP terahertz parametric oscillator to decrease the thermal effect and increase the fundamental beam size. The surface-emitted output method for the terahertz wave was used to extract the THz wave efficiently. Additionally, a non-collinear convex-plane fundamental cavity was adopted to further offset the thermal effect and increase the fundamental beam size. Finally, the obtained maximum average THz output power was 367 μW at 3.88 THz when the PRF was 7 kHz and the diode pump power was 105 W. As far as we know, 367 μW is the highest average THz power for SPS sources. The SE configuration is adopted to efficiently extract the THz wave.

2. Experimental Setup

The experimental schematic of the diode-side-pumped intracavity SPS laser is shown in Fig. 1. The fundamental cavity was composed of M1, M2, and the total reflection surface of the RTP crystal. The cavity was designed as a convex-plane configuration so that the thermal effect could be offset in some degree and the fundamental beam size could be further increased. The length of the whole fundamental cavity was 330 mm. The mirror M1 was convex and the curvature radius was 2000 mm. It was high reflection (HR) coated at 1064 nm (R>99.99%). The output mirror M2 was flat with a reflectivity of 99.54% at 1064 nm. Diode-side-pumping for the gain medium
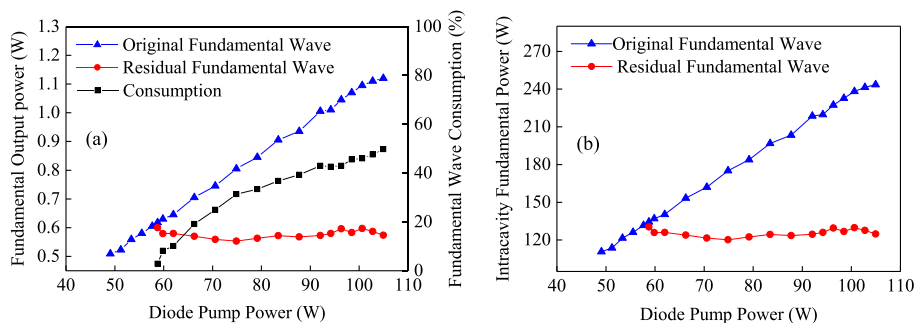
Fig. 3. Variations of the (a) fundamental output power and (b) intracavity fundamental power with the diode pump power.

Nd:YAG was adopted. The maximum diode laser power was 180 W. The Nd:YAG rod was 65 mm in length and 3 mm in diameter, and was antireflection (AR) coated at 1064 nm on both ends. An acousto-optic (AO) module (Gooch & Housego Company) was used to obtain the Q-switched pulses with high frequency rate. The Stokes resonator was a plane-plane configuration including mirrors M3 and M4. In order to prevent the Stokes cavity from clipping the fundamental beam, the mirrors M3 and M4 were both fabricated as the semicircle shape. M3 was HR coated in the range of 1060–1100 nm, and M4 was the output mirror of the Stokes resonator. The Stokes cavity length was 120 mm. The RTP crystal was isosceles trapezoid shape in the *x-y* plane with the base-angle of 60°. By this design, the THz beam could nearly perpendicularly radiate through the base-surface of the crystal without the need of any other couplers. The baseline and waist of the RTP crystal in the *x-y* plane were 18 mm and 10 mm, respectively. The thickness of the RTP crystal was 5 mm. Two waist-surfaces of the RTP crystal were both AR coated in the range of 1060–1100 nm. M3 and M4 were installed on two independent dynamoelectric rotating-platforms, respectively. The oscillating direction of the Stokes wave could be precisely adjusted by controlling the rotating-platforms. Thereby, the tunings of the Stokes wavelength and the THz frequency were realized. The average THz output power was recorded by a calibrated Golay detector (TYDEX GC-1D). To eliminate the interference of the undesired near-IR and background waves, a long pass filter (TYDEX LPF 14.3-47) was installed in front of the Golay cell. An optical chopper with the duty cycle of 50% and the operation frequency of 10 Hz was placed between the RTP crystal and the Golay cell.

3. Experimental Results and Discussions

The angle-tuning characteristic of the RTP crystal has been investigated in the external-cavity pumped SPS source [20]. The THz-frequency tuning range of a certain nonlinear crystal is mainly related to the crystal's properties and is hardly affected by the pumping configuration. The optimal THz frequency based on the RTP crystal was at 3.88 THz where the THz output power was maximal. The pulse repetition frequency was selected as 7 kHz. The output power scaling properties of the fundamental wave before and after consumption for the diode-side-pumped SPS laser at 3.88 THz are investigated and shown in Fig. 3(a). By intentionally aligning and misaligning the mirror M4, the SPS process could be switched on and off. When the SPS process was switched off, the fundamental output power scaled linearly with increasing diode power. When the SPS process was switched on, the fundamental wave began to be consumed for the incident diode pump power above 58 W. With further increasing the diode pump power, the residual fundamental output power was clamped at an average level of 570 mW. But the fundamental consumption (the difference power between the original fundamental and residual fundamental waves divided by the original fundamental wave power) increased nearly linearly, indicating that the fundamental wave was consumed by the SPS process. This phenomenon that once the SPS starts, the residual
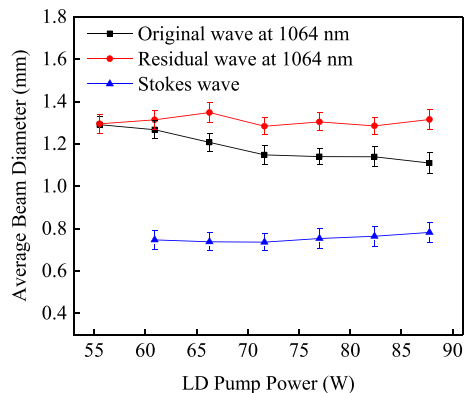
Fig. 4. Beam diameters of the original fundamental, residual fundamental and stokes waves inside the RTP crystal as a function of the diode pump power.

fundamental power remains nearly constant and all the additional power is transferred is common in the terahertz parametric oscillator [26] and also happens in other nonlinear effects such as stimulated Raman scattering [38]. We will investigate the physical essence of this effect in the future work using rate equations. Finally, the fundamental output powers before and after consumption were measured as 1.12 W and 574 mW respectively, and the corresponding fundamental wave consumption was calculated as 49% when the diode pump power was 105 W. Fig. 3(b) shows the intracavity fundamental power as a function of diode pump power. It is the result of the output power divided by the M2 transmittance (T = 0.46%). The fundamental threshold of the SPS process in the RTP diode-side-pumped system was calculated as 132 W. The maximum one-way fundamental powers in the cavity before and after consumption were calculated as 243 W and 124 W, respectively.

As mentioned above, the non-collinear phase matching condition must be satisfied in the SPS process. The spatial interaction between the fundamental and Stokes waves in a linear crystal is shown in the area I in Fig. 1. The diagram is sketched for the linear geometry just for easier understanding. The interacting area is same for a surface-emitted configuration because of the mirror reflection. The fundamental beam was perpendicularly incident into the crystal. The Stokes beam oscillated with an angle φ from the fundamental beam according to the near-forward Raman scattering configuration $X(ZZ)X+\varphi$ in the SPS process. The THz beam was generated in the overlapping area I. Obviously, the larger the fundamental beam size is, the larger the interaction volume between the fundamental and Stokes waves will be in the nonlinear crystal.

The fundamental beam sizes (before and after consumption) and the Stokes beam sizes inside the RTP crystal under different diode pump powers were then investigated. The original fundamental beam sizes outside the oscillator were firstly measured using a camera beam profiler (THORLABS, BC106N-VIS/M, 350–1100 nm) when the SPS was switched off. The beam radii at different positions were fitted into the curve $\omega^2(x) = \omega_0^2[1 + (x/f)^2]$, where x represents the distance between the output coupler mirror and the camera beam profiler, ω_0 is the beam waist radius, $f = \pi\omega_0^2/(\lambda M^2)$ is called the Rayleigh length, M^2 is the beam quality parameter. Then the ABCD modeling was used to deduce the original fundamental beam size inside the RTP crystal. When the SPS was switched on, the fundamental wave was consumed and the Stokes and THz waves were generated. The residual fundamental size and the Stokes beam size inside the RTP crystal could also be calculated. The fundamental (before and after consumption) and Stokes beam sizes inside the RTP crystal as functions of diode pump powers are shown in Fig. 4. The fundamental beam size decreased slightly with increasing diode power when the SPS was switched off, and it became larger after consumption. The generated Stokes beam size increased slightly with increasing diode power. The average fundamental beam diameters before and after consumption were about 1.2 and 1.3 mm, respectively. The average Stokes beam diameter was about 0.8 mm.
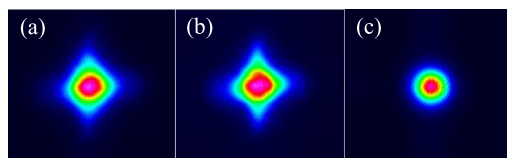
Fig. 5. Mode profiles of the (a) original fundamental, (b) residual fundamental and (c) stokes waves.
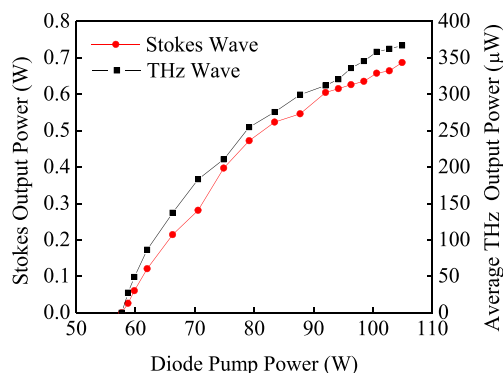

Fig. 6. The input-output characteristics of the Stokes and THz waves.

The beam profiles of the fundamental (before and after consumption) and generated Stokes waves are shown in Fig. 5 when the diode pump power was 85 W. Because of the diode-side-pumped configuration, the beam quality of the original fundamental wave was not very good. The mode structure of the fundamental wave became a little degraded after the terahertz wave was generated. In contrast, the beam quality of the Stokes wave was much better. And there was no obvious change in the Stokes mode profile with increasing diode pump power. This phenomenon was similar to the beam-cleanup effect [37] occurred in the general Raman lasers that although the fundament wave oscillated on multiple transverse modes, the generated Raman wave could oscillate as near diffraction-limited. The horizontal and vertical beam quality parameters of Stokes wave were measured as 1.24, and 1.25 respectively using an M^2 beam quality analysis system (THORLABS, M2MS, 400–5000 nm).

The input-output characteristics of the Stokes and THz waves are demonstrated in Fig. 6. The Stokes and THz waves were generated simultaneously when the incident diode pump power was 58 W. With increasing diode pump power, their average output powers increased nearly linearly in the beginning but tended to saturate for high diode pump power. The saturation may be caused in a way by the thermal effect. The average THz output power increased up to 367 μW when the diode pump power was 105 W. Higher diode pump power was not tried considering the optical damage threshold of RTP. The diode-to-THz conversion efficiency is lower compared to that in the diode-end-pumped configuration due to the insufficient absorption of the diode pump light in the outer part of the laser rod. However, the terahertz average power of 367 μW is the highest for SPS sources as far as we know (triple of the highest power ever reported for the SPS lasers).

The pulse temporal behavior could visually describe the fundamental wave consumption and the Stokes wave generation. The fundamental and Stokes pulses under different diode pump powers were detected using two same Si detectors (THORLABS, DET10A/M, 400–1100 nm). The waveforms were recorded by an oscilloscope (Tektronic TDS5052B, 500MHz, 5GS/s), as shown in Fig. 7. The fundamental wave had no depletion and the pulse width was 202 ns when the diode power was 55 W which was under the SPS threshold, as shown in Fig. 7(a). When the diode power was 70 W, the fundamental wave had obvious depletion (residual pulse width was 147 ns), as shown in Fig. 7(b). The Stokes pulse was generated and the rising edge corresponded to the point where the fundamental pulse depletion commenced. The Stokes pulse width was 42 ns. With increasing diode power, the residual fundamental pulse width decreased, and the depletion of the
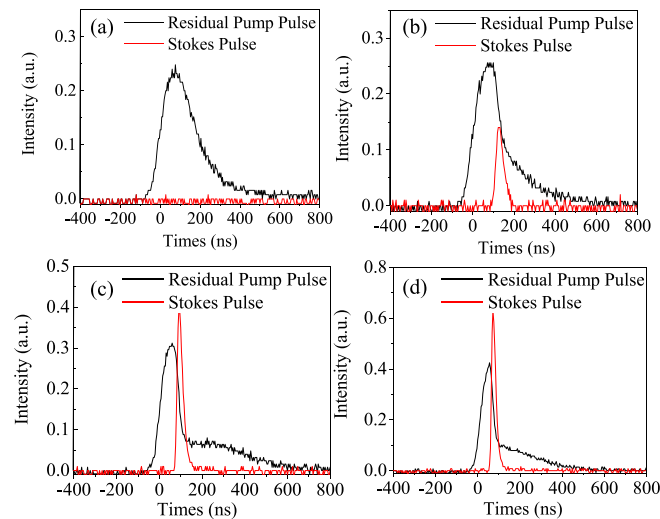
Fig. 7. Waveforms of the fundamental and Stokes pulses when the diode pump powers were (a) 55 W, (b) 70 W, (c) 85 W, and (d) 100 W, respectively.
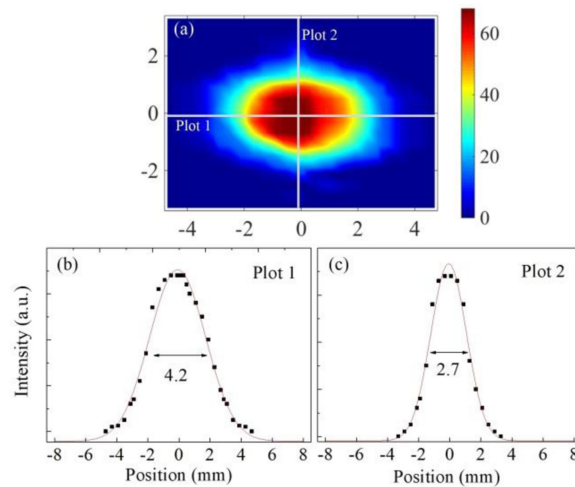

Fig. 8. (a) Two-dimensional THz beam pattern measured at 2 cm far from the output surface. (b), (c) THz beam intensity distributions in the horizontal and vertical directions.

fundamental wave was more serious. The pulse widths of the residual fundamental and Stokes waves were 93 ns and 33 ns respectively when the diode power was 85 W, as shown in Fig. 7(c), and 67 ns and 21 ns respectively when the diode power was 100 W, as shown in Fig. 7(d).

The THz beam profile of the SE intracavity diode-side-pumped system was measured by adopting the approach of two-dimensional scanning. A silver paper with a 200 μm diameter pinhole was stick in front of the Golay cell entrance window. The THz beam pattern that was measured at 2 cm far from the THz output surface is shown in Fig. 8(a). The measured THz spot had an asymmetric elliptical distribution which was caused by the elliptical fundamental beam shape on the output surface. The THz wave had a close-to-Gaussian distribution both in the horizontal and vertical directions as shown in Figs. 8(b) and (c) (The solid lines were Gaussian fitted). The half maximum (FWHM) beam diameters were measured as 4.2 mm in horizontal direction and 2.7 mm in vertical direction, respectively.

4. Conclusion

A high average power intracavity SPS laser based on RTP crystal has been demonstrated. The SE configuration is adopted to efficiently extract the THz wave. The diode side pumping for the gain medium Nd:YAG is adopted to obtain a high intracavity fundamental power and a large fundamental beam size. A non-collinear convex-plane fundamental cavity is employed so that the thermal effect can be offset in some degree and the fundamental beam size can be further increased. The fundamental beam diameters before and after consumption in the RTP crystal are about 1.2 and 1.3 mm, respectively. When the diode pump power is 105 W and the PRF is 7 kHz, the obtained maximum average THz power is 367 μW at 3.88 THz. Although the diode-to-THz conversion efficiency is lower compared to that in the diode-end-pumped configuration, as far as we know, the THz output power of 367 μW is the highest for terahertz parametric sources based on SPS.

References

[1] S. J. Oh *et al.*, "Molecular imaging with terahertz waves," *Opt. Express*, vol. 19, no. 5, pp. 4009–4016, 2011.

[2] F. M. Al-Douseri, Y. Chen, and X.-C. Zhang, "THz wave sensing for petroleum industrial applications," *Int. J. Infrared Millim. Waves*, vol. 27, no. 4, pp. 481–503, 2007.

[3] A. G. Davies, A. D. Burnett, W. H. Fan, E. H. Linfield, and J. E. Cunningham, "Terahertz spectroscopy of explosives and drugs," *Mater. Today*, vol. 11, no. 3, pp. 18–26, 2008.

[4] G. Kim, J. Kim, S. Jeon, J. Kim, K. Park, and C. Oh, "Enhanced continuous-wave terahertz imaging with a horn antenna for food inspection," *J. Infrared Milli. THz Waves*, vol. 33, no. 6, pp. 657–664, 2012.

[5] M. C. Kemp, P. F. Taday, B. E. Cole, J. A. Cluff, A. J. Fitzgerald, and W. R. Tribe, "Security applications of terahertz technology," *Proc. SPIE*, vol. 5070, pp. 44–52, 2003.

[6] K. Ajito, Y. Ueno, "THz chemical imaging for biological applications," *IEEE Trans. Terahertz Sci. Technol.*, vol. 1, no. 1, pp. 293–300, 2011.

[7] K. Kawase, M. Sato, T. Taniuchi, H. Ito, "Coherent tunable THz-wave generation from $LiNbO_3$ with monolithic grating coupler," *Appl. Phys. Lett.*, vol. 68, no. 18, pp. 2483–2485, 1996.

[8] K. Kawase, J. Shikata, and H. Ito, "Terahertz wave parametric source," *J. Phys. D Appl. Phys.*, vol. 35, no. 3, pp. R1–R14, 2002.

[9] J. Shikata, K. Kawase, K. Karino, T. Taniuchi, and H. Ito, "Tunable terahertz-wave parametric oscillators using $LiNbO_3$ and $MgO:LiNbO_3$ crystals," *IEEE Trans. Microw. Theory Tech.*, vol. 48, no. 4, pp. 653–661, 2000.

[10] K. Imai, K. Kawase, H. Minamide, and H. Ito, "Achromatically injection-seeded terahertz-wave parametric generator," *Opt. Lett.*, vol. 27, no. 24, pp. 2173–2175, 2002.

[11] B. Sun, S. Li, J. Liu, E. Li, and J. Yao, "Terahertz-wave parametric oscillator with a misalignment-resistant tuning cavity," *Opt. Lett.*, vol. 36, no. 10, pp. 1845–1847, 2011.

[12] R. Zhang, Y. Qu, W. Zhao, C. Liu, and Z. Chen, "Si-prism-array coupled terahertz-wave parametric oscillator with pump light totally reflected at the terahertz-wave exit surface," *Opt. Lett.*, vol. 41, no. 17, pp. 4016–4019, 2016.

[13] Z. Yang *et al.*, "High-energy terahertz wave parametric oscillator with a surface-emitted ring-cavity configuration," *Opt. Lett.*, vol. 41, pp. 2262–2265, 2016.

[14] W. Wang *et al.*, "Terahertz parametric oscillator based on $KTiOPO_4$ crystal," *Opt. Lett.*, vol. 39, no. 13, pp. 3706–3709, 2014.

[15] W. Wang *et al.*, "THz-wave generation via stimulated polariton scattering in $KTiOAsO_4$ crystal," *Opt. Express*, vol. 22, no. 14, pp. 17092–17098, 2014.

[16] T. A. Ortega, H. M. Pask, D. J. Spence, and A. J. Lee, "Stimulated polariton scattering in an intracavity $RbTiOPO_4$ crystal generating frequency-tunable THz output," *Opt. Express*, vol. 24, no. 10, pp. 10254–10264, 2016.

[17] M. V. Pack, D. J. Armstrong, and A. V. Smith, "Measurement of the $\chi^{(2)}$ tensors of $KTiOPO_4$, $KTiOAsO_4$, $RbTiOPO_4$, and $RbTiOAsO_4$ crystals," *Appl. Opt.*, vol. 43, no. 16, pp. 3319–3323, 2004.

[18] A. Hildenbrand, F.R. Wagner, J.-Y. Natoli, and M. Commandré, "Nanosecond laser induced damage in $RbTiOPO_4$: The missing influence of crystal quality," *Opt. Express*, vol. 17, no. 20, pp. 18263–18270, 2009.

[19] T. A. Ortega, H. M. Pask, D. J. Spence, and A. J. Lee, "Tunable 3-6 THz polariton laser exceeding 0.1 mW average output power based on crystalline $RbTiOPO_4$," *IEEE J. Sel. Topics Quantum Electron.*, vol. 24, no. 5, pp. 1–6, Sep. 2018.

[20] F. Gao *et al.*, "Terahertz parametric oscillator with the surface-emitted configuration in $RbTiOPO_4$ crystal," *Opt. Laser Technol.*, vol. 104, no. 1, pp. 37–42, 2018.

[21] T. Ikari, X. B. Zhang, H. Minamide, and H. Ito, "THz-wave parametric oscillator with a surface-emitted configuration," *Opt. Express*, vol. 14, no. 4, pp. 1604–1610, 2006.

[22] W. Wang *et al.*, "Multiple-beam output of a surface-emitted terahertzwave parametric oscillator by using a slab $MgO:LiNbO_3$ crystal," *Opt. Lett.*, vol. 39, no. 4, pp. 754–757, 2014.

[23] G. Tang *et al.*, "Energy scaling of terahertz-wave parametric sources," *Opt. Express*, vol. 23, no. 4, pp. 4144–4152, 2015.

[24] T. J. Edwards, D. Walsh, M. B. Spurr, C. F. Rae, M. H. Dunn, and P. G. Browne, "Compact source of continuously and widely-tunable terahertz radiation," *Opt. Express*, vol. 14, no. 4, pp. 1582–1589, 2006.

[25] D. J. M. Stothard *et al.*, "Line-narrowed, compact, and coherent source of widely tunable terahertz radiation," *Appl. Phys. Lett.*, vol. 92, no. 14, 2008, Art. no. 141105.

[26] A. Lee, Y. He, and H. Pask, "Frequency-tunable THz source based on stimulated polariton scattering in Mg: $LiNbO_3$," *IEEE J. Quantum Electron.*, vol. 49, no. 3, pp. 357–364, Mar. 2013.

[27] T. Ortega, H. Pask, D. Spence, and A. Lee, "THz polariton laser using an intracavity $Mg:LiNbO_3$ crystal with protective Teflon coating," *Opt. Express*, vol. 25, no. 4, pp. 3991–3999, 2017.

[28] S. C. Tidwell, J. F. Seamans, M. S. Bowers, and A. K. Cousins, "Scaling CW diode-end-pumped Nd:YAG lasers to high average powers," *IEEE J. Quantum Electron.*, vol. 28, no. 4, pp. 997–1009, Apr. 1992.

[29] M. P. Murdough and C. A. Denman, "Mode-volume and pump-power limitations in injection-locked TEM_{00} Nd:YAG rod lasers," *Appl. Opt.*, vol. 35, no. 30, pp. 5925–5936, 1996.

[30] T. Kojima and K. Yasui, "Efficient diode side-pumping configuration of a Nd:YAG rod laser with a diffusive cavity," *Appl. Opt.*, vol. 36, no. 21, pp. 4981–4984, 1997.

[31] D. Golla *et al.*, "300-W cw diode-laser side-pumped Nd: YAG rod laser," *Opt. Lett.*, vol. 20, no. 10, pp. 1148–1150, 1995.

[32] J. Yi, H. J. Moon, and J. Lee, "Diode-pumped 100-W green Nd:YAG rod laser," *Appl. Opt.*, vol. 43, no. 18, pp. 3732–3737, 2004.

[33] S. Li *et al.*, "Diode-side-pumped intracavity frequency-doubled Nd: $YAG/BaWO_4$ Raman laser generating average output pow of 3.14 W at 590 nm," *Opt. Lett.*, vol. 32, no. 20, pp. 2951–2953, 2007.

[34] C. Y. Li *et al.*, "106.5 W high beam quality diode-side-pumped Nd:YAG laser at 1123 nm," *Opt. Express*, vol. 18, no. 8, pp. 7923–7928, 2010.

[35] S. Konno, S. Fujikawa, and K. Yasui, "80W cw TEM_{00} 1064 nm beam generation by use of a diode-side-pumped Nd:YAG rod laser," *Appl. Phys. Lett.*, vol. 70, no. 20, pp. 2650–2651, 1997.

[36] W. Xie *et al.*, "Fluorescence feedback control of an active Q-switched diode-pumped Nd:YVO4 laser," *Appl. Opt.*, vol. 39, no. 30, pp. 978–981, 2000.

[37] J. T. Murray, W. L. Austin, and R. C. Powell, "Intracavity Raman conversion and Raman beam cleanup," *Opt. Mater.*, vol. 11, no. 4, pp. 353–371, 1999.

[38] Y. Chang, Y. Huang, K. Su, and Y. Chen, "Diode-pumped multi-frequency Q-switched laser with intracavity cascade Raman emission," *Opt. Express*, vol. 16, no. 11, pp. 8286–8291, 2008.